ARTICLES
PUBLISHED ONLINE: 6 JULY 2015 | DOI: 10.1038/NNANO.2015.137
nature nanotechnology

# Controlled steering of Cherenkov surface plasmon wakes with a one-dimensional metamaterial

Patrice Genevet[1,2*†], Daniel Wintz[1†], Antonio Ambrosio[1,3†], Alan She[1], Romain Blanchard[1,4] and Federico Capasso[1,4*]

**In the Cherenkov effect a charged particle moving with a velocity faster than the phase velocity of light in the medium radiates light that forms a cone with a half angle determined by the ratio of the two speeds. Here, we show that by creating a running wave of polarization along a one-dimensional metallic nanostructure consisting of subwavelength-spaced rotated apertures that propagates faster than the surface plasmon polariton phase velocity, we can generate surface plasmon wakes, a two-dimensional analogue of Cherenkov radiation. The running wave of polarization travels with a speed determined by the angle of incidence and the photon spin angular momentum of the incident radiation. By changing either one of these properties we demonstrate controlled steering of the Cherenkov surface plasmon wakes.**

As an accomplished sailor, Lord Kelvin was fascinated by the marvelous yet complex wave patterns generated behind his boat on the water's surface. He realized that his boat was always ahead of the waves that it creates[1], generating a wave pattern of two lines that form the arms of a V, with the boat giving rise to the wake at the apex. In shallow water, the angle $\gamma$ between the boat trajectory and the wake is given by the relation $\sin\gamma = c/U$, where $c$ is the speed of the surface wave and $U$ is the speed of the boat. In fact, this is a general wave phenomenon—wakes are formed each time a perturbation travels faster than the phase velocity of the waves it creates, accounting for phenomena as diverse as sonic booms and Cherenkov radiation. The latter occurs when a charged particle (such as an electron) moves at a velocity faster than the phase velocity of light in that medium. Microscopically, the moving charge induces a trail of polarization by interacting with polarizable dipoles in the medium. On returning to equilibrium, the induced dipoles re-radiate immediately after the electron has passed the interaction zone[2]. (Note that the particle itself is not radiating, and only the response of the medium produces the secondary waves forming the Cherenkov radiation.)

Combining Cherenkov physics with the concept of artificial optical materials, Veselago predicted that the wake of the Cherenkov radiation would be directed backwards relative to the motion of the charged particles in negative-index materials[3]. This effect has been demonstrated experimentally with microwaves and promises the development of Cherenkov counters with higher efficiency[4,5], as well as novel high-power electric devices with miniaturization and higher efficiency[6]. In ref. 5, the authors show that a moving charged particle can be accurately modelled by a phased dipole array consisting of an infinite number of dipoles situated along the trajectory of the moving charge. More precisely, they demonstrate that the current density of a moving charge is very similar to the current density of a phased dipole array. Indeed, the only noticeable difference is that the charged particle emits a spectrum of frequencies. Other unusual Cherenkov emissions related to the Smith–Purcell effect have been reported for charged particles propagating in or near periodic media[7,8] such as photonic crystals[9] and other types of periodic inhomogeneous or anisotropic media[10–14]. Here, we show that a one-dimensional array of nanostructures can excite and steer surface plasmon wakes via a mechanism analogous to Cherenkov radiation.

## A long slit as the introductory case

Consider a light beam polarized perpendicular to a slit etched in a thin metal film and incident at an angle $\theta$. As analysed by Lee and colleagues[15], this beam will induce a polarization along the slit. If $\theta = 0°$ and the slit is long compared to $\lambda_{SPP}$, the slit will radiate surface plasmon polariton (SPP) plane waves that propagate with a wavevector normal to the slit. However, if the light is polarized perpendicular to the plane of incidence (S-polarized) and impinges obliquely at an angle $\theta$ (Fig. 1a), the light creates a running wave of polarization (RWP) with an amplitude that varies sinusoidally along the slit with a wavelength $\lambda_{RWP} = (\lambda_0/\sin\theta)$, as indicated in Fig. 1b, where $\lambda_0$ is the free-space wavelength. The phase velocity of the RWP is $c_{RWP} = (\lambda_{RWP}/2\pi)\omega_0 = c/\sin\theta$ where $c$ is the speed of light in vacuum and $\omega_0$ is the frequency. Note that at normal incidence ($\theta = 0°$), $c_{RWP}$ is infinite and all the dipoles are excited together in phase. An example of the electric field component normal to the slit in the vicinity of the surface calculated by finite-difference time-domain (FDTD) simulation is shown in Fig. 1c.

The RWP can be understood as a series of dipoles oriented normal to the slit axis, distributed along the slit with a phase profile given by $\phi(x) = (2\pi/\lambda_0)x\sin\theta$, which propagates along $x$ at a velocity $c_{RWP}$. As can be seen in Fig. 1c, the RWP excites SPPs, which constructively interfere along the dashed lines, creating wakes defined by the angle $\gamma$. The angle of the wakes can be derived by imposing the condition that the propagation phase shift $((2\pi/\lambda_0)\sin\theta\,\Delta x_0)$ between two light rays of the incident wavefront at an angle $\theta$, impinging on the surface at points separated by a distance $\Delta x_0$, is exactly compensated by the phase shift $((2\pi/\lambda_{SPP})\sin\gamma\,\Delta x_0)$ between SPP wakes propagating out of those points. This yields

$$\sin\gamma = \frac{c_{SPP}}{c_{RWP}} = \frac{\sin\theta}{n_{eff}} \quad (1)$$

[1]School of Engineering and Applied Sciences, Harvard University, 9 Oxford Street, McKay 125, Cambridge, Massachusetts 02138, USA. [2]Singapore Institute of Manufacturing Technology, 71 Nanyang Drive, Singapore 638075, Singapore. [3]CNR-SPIN U.O.S. Napoli, Dipartimento di Fisica, Complesso Universitario di Monte Sant'Angelo, Università di Napoli Federico II, Via Cintia, Napoli 80126, Italy. [4]Eos Photonics Inc., 30 Spinelli Place, Cambridge, Massachusetts 02138, USA. †These authors contributed equally to this work. *e-mail: genevetp@simtech.a-star.edu.sg; capasso@seas.harvard.edu

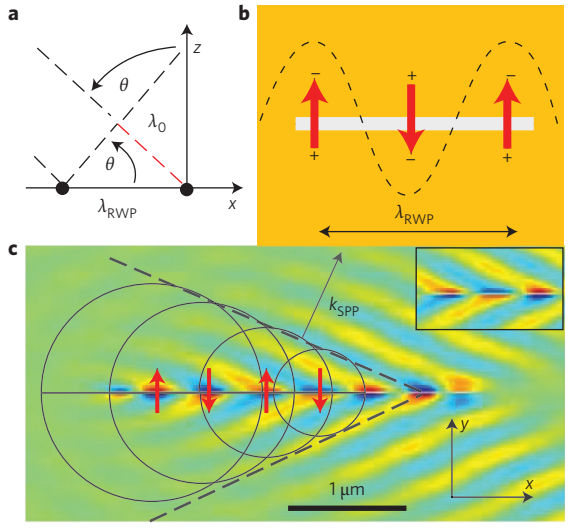


**Figure 1 | Excitation of Cherenkov surface plasmon wakes with a running wave of polarization. a**,**b**, Light impinging on a slit in a metal film at oblique incidence $\theta$ with free-space wavelength $\lambda_0$ generates a RWP of wavelength $\lambda_{RWP} = (\lambda_0/\sin\theta)$, which propagates with a phase velocity $c_{RWP} = (c/\sin\theta) > c_{SPP}$, where $c$ is the phase velocity of light in free space and $c_{SPP}$ is the SPP phase velocity. The red dashed line denotes an extra path length of one free-space wavelength, such that the light incident at the black dots has the same phase. **c**, FDTD simulation showing the real part of the electric field normal ($z$ axis) to the slit ($x$ axis) 5 nm above the surface. The slit (3 μm long and 50 nm wide) is excited at visible wavelength (610 nm) by a beam incident at $\theta = 30°$. The superimposed circles are the Huygens' representation of the surface waves centred at selected dipoles. It shows the RWP that generates the SPPs, which interfere to form wakes at an angle $\gamma$ that follows the Cherenkov equation, $\sin\gamma = (c_{SPP}/c_{RWP})$. Inset: zoomed-in view of the slit.

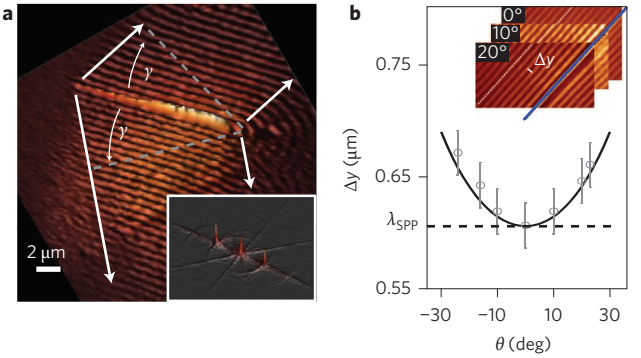


**Figure 2 | Near-field scanning optical microscopy data for surface plasmon wakes created along a long slit etched in a metal film. a**, Three-dimensional rendering of an experimental near-field scanning optical image of the interference pattern of surface plasmon wakes propagating and a beam incident at an angle of $\theta = 23°$. $\gamma$ is the angle of wake propagation with respect to the slit axis. The fringes result from the interference pattern of the surface plasmons and the incident light that is transmitted through the thin gold film. The fringes are parallel to the slit but the surface plasmons propagate at an angle relative to the slit (Supplementary Fig. 1). White arrows indicate the wavevector of the surface plasmon wakes, and the grey dashed lines denote the wavefront. Inset: spatial Fourier transform of main image which is used to calculate the period of the interference pattern. **b**, Evolution of the period of the interference pattern as a function of $\theta$. The solid line is the expected theoretical value from equation (2); its minimum corresponds to the surface plasmon wavelength, $\lambda_{SPP} = (\lambda_0/n_{eff})$. Inset: measured interference patterns for different angles $\theta$. The blue line in the inset represents the position of the slit for all three images. The distance between the white dashed line and the slit in each image corrreponds to $7\Delta y$, providing a visualization of the change in fringe separation with angle of incidence. Error bars in $\Delta y$ are computed as the FWHM of the peaks in the Fourier transform in the inset of **a**.

where $n_{eff} = (\lambda_0/\lambda_{SPP}) = [(\varepsilon_{air}\varepsilon_{metal})/(\varepsilon_{air} + \varepsilon_{metal})]^{1/2}$ is the effective index of the SPP mode on a metal/air interface. Note that $n_{eff}$ always exceeds unity and the SPP dispersion curve is below the light-line. The condition for generating SPP wakes, $c_{RWP} = (c/\sin\theta) > c_{SPP}$, is thus satisfied for any $\theta$.

We experimentally analysed the angle of surface plasmon wakes from a slit as a function of the angle of incidence with a near-field scanning optical microscope (NSOM) (Supplementary Fig. 3). To access not only the intensity, but also the phase profile of SPPs propagating on the metal film, we used a ~50-nm-thick gold film, template stripped[16] from a silicon wafer. The film thickness allows a fraction of the incident free-space light to be transmitted through the film and interfere with the SPPs propagating along the gold/air interface. The light intensity collected at each point of the NSOM scan is the interference of the electric field of the incident light and the SPP field generated by the slit. An example of the resulting interference is presented in Fig. 2a. From this interference pattern we can extract the angle of propagation $\gamma$ of the SPP wakes. Although the wakes are generated at an angle $\gamma$ given by equation (1), the fringes are parallel to the slit due to the interference of the SPP wake and the obliquely incident beam that is transmitted through the thin gold film (Supplementary Sections 1 and 3). Through geometric analysis, we derive the angle of the SPP wake from the period of the intensity modulation, $\Delta y = \lambda_0/(n_{eff}\cos\gamma)$. Combining this expression with equation (1), we obtain the separation of the fringes as a function of the angle of incidence:

$$\Delta y = \frac{\lambda_0}{\sqrt{n_{eff}^2 - (\sin\theta)^2}} \qquad (2)$$

The solid line in Fig. 2b represents the calculated $\Delta y$ expressed in terms of $\theta$ using equation (2). To extract the experimental value of $\Delta y$, we compute the spatial Fourier transform of the NSOM scans (Fig. 2a, inset) and compare the results with the expression above (Fig. 2b).

## 1D metamaterial gives a controllable phase term

Metasurfaces made of arrays of optical resonators (for example, antennas) have been widely investigated[17–21]. In our experiment, we use a one-dimensional metagrating made of elements that introduce a linear phase shift along the trajectory of the RWP. This extra phase shift $\Delta\phi$ is imposed by fabricating aperture antennas in a line, separated by a distance that is small compared to $\lambda_{SPP}$. With these local phase shifts along the trajectory of the RWP, we modify the radiation angle $\gamma$ of the SPP wakes. A plane wave incident on the surface at an angle $\theta$ will excite SPPs in adjacent antennas, which will constructively interfere at an angle $\gamma$ given by the condition that the phase shifts associated with optical paths of adjacent antennas are equal. From Fig. 3a, one can see that this condition can be written as

$$k_0 \sin\theta\,\Delta x + \Delta\phi = k_{SPP}\sin\gamma\,\Delta x \qquad (3)$$

The first term in equation (3) represents the relative phase shift due to the plane wave's oblique incidence $\theta$ on two adjacent apertures separated by $\Delta x$ ($\ll\lambda_0$) (Fig. 3a). The term on the right-hand side of the equation represents the phase shift between the SPP waves emerging from the two antennas, and $\Delta\phi$ is the phase difference introduced by the one-dimensional

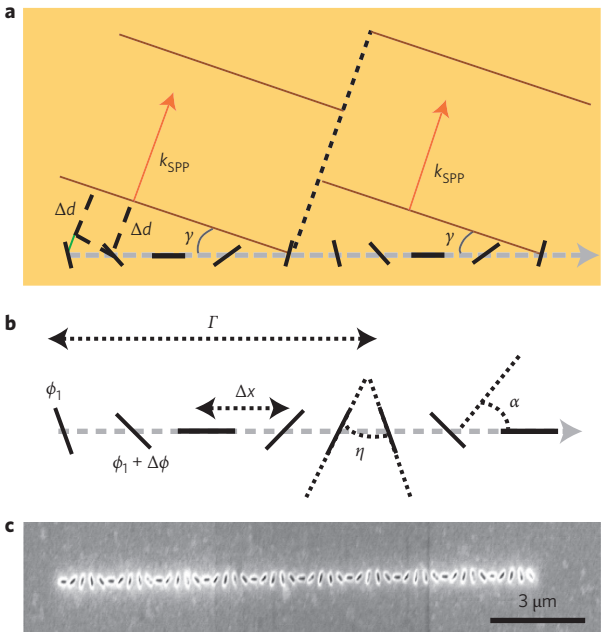


**Figure 3 | Creation of SPP wakes by a one-dimensional metamaterial and scanning electron micrograph of the nanostructure. a**,**b**, Schematic representations of the creation of SPP wakes by a one-dimensional array of aperture antennas (black bars) designed to generate a phase change with constant phase gradient ($\Delta\phi/\Delta x$) in the emission of SPPs. The one-dimensional phased array is excited by light incident on the surface at an angle $\theta$, creating a RWP denoted by the grey dashed arrow. In **a**, the SPP propagation path length difference between adjacent antennas is shown in green (corresponding to the right-hand side of equation (3)). Note that each antenna period, denoted by $\Gamma$ in **b**, creates its own wake (brown lines), which arises from the constructive interference of the wavelets originating from each antenna within the period. The angle of the wake, $\gamma$, depends on the angle of incidence (equation (4)), where positive (negative) $\gamma$ corresponds to a wake wavevector propagating to the right (left). The dashed black line in **a** corresponds to the zero intensity alleys separating the wakes generated by adjacent periods. **b**, Angle $\gamma$ can be controlled by changing $\Delta\phi$, which is proportional to the spatial rotation rate of the antennas ($d\alpha(x)/dx = \Delta\phi/\Delta x = (\pi/\Gamma)$. $\eta$ is the rotation step and $\alpha$ is the angle above the horizontal. **c**, Scanning electron micrograph of the nanostructures used to generate the SPP wakes. The apertures are created by focused ion beam milling.

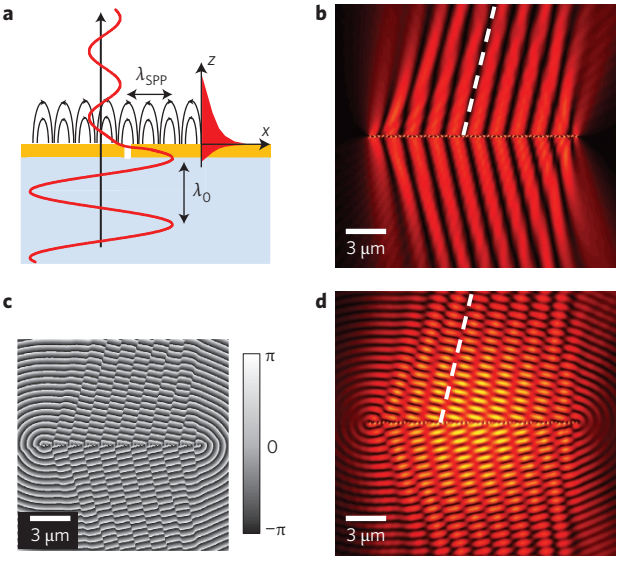


**Figure 4 | Analytical model treating the rotated nanoslits as a phased dipole array, including interference between the SPP wakes and the incident beam. a**, Light incident on an aperture excites SPPs, and some light transmits through the thin gold film. **b**,**c**, Calculated intensity (**b**) and phase distribution (**c**) of SPPs generated by a phased array (rotated apertures) with $\Gamma = 1.5$ μm excited by right circularly polarized light. The imparted phase from the rotation of the apertures varies from 0 to π along each period, creating alleys of high intensity separated by lines of zero intensity. Simpler geometries are presented in Supplementary Figs 4 and 5. **d**, Simulated interference pattern between the SPPs and the transmitted beam for normal incidence. The white dashed line represents the alley where the SPP electric field is zero, and the intensity is that of the transmitted beam. These lines are parallel to the direction of propagation of the wakes. A comparison of the analytical model and an FDTD computation is presented in Supplementary Fig. 7.

phased array (Fig. 3a). Taking the limit $\Delta x \to 0$ yields the relation

$$\sin\gamma = \frac{\sin\theta}{n_{\text{eff}}} + \frac{1}{k_{\text{SPP}}}\frac{\mathrm{d}\phi}{\mathrm{d}x} \quad (4)$$

Note that the wakes can be made to propagate either forwards or backwards with respect to the RWP depending on the relative magnitude of the terms on the right-hand side of equation (4).

By replacing the slit discussed above with the ensemble of rotating linear apertures of Fig. 3, we experimentally demonstrate the ability to route the SPP wakes in different directions by introducing local phase shifts. As has been discussed recently, there are different ways to achieve local phase shifts[22–24]. Here, we use the geometric phase shift (often called the Pancharatnam–Berry phase) imparted to the SPPs by the interaction of elliptically or circularly polarized light with anisotropic aperture antennas.

Consider normally incident light with linear polarization. Even if the antennas are rotated sequentially, all of the apertures are excited in phase (with different amplitudes that depend on the projection of the polarization onto the axis normal to the aperture). This scenario does not allow us to introduce a local phase shift from the rotation of the apertures. On the other hand, circularly or elliptically polarized light has a phase delay between the $x$ and $y$ components and this phase delay introduces a dephasing in the excitation of the rotated apertures. Under this illumination condition, coupling to SPPs at a nanoslit depends on the electric field component perpendicular to the nanoslit ($E_x \cdot \hat{n} + E_y \cdot \hat{n}$, where $\hat{n}$ is the unit vector perpendicular to the nanoslit). For circularly polarized light, this field projection is constant in amplitude with respect to the orientation of the nanoslit; however, its phase depends linearly on the nanoslit rotation angle. Therefore, by simply rotating each nanoslit, one by one with respect to the others, a progressive phase delay in SPP emission can be imposed (Supplementary Figs 2 and 8 and Supplementary Section 2.2). This phase shift combines with the phase shift associated with the angle of incidence to modify the emission angle of the SPP wakes[22,23]. Because of both their local orientation (Fig. 3b) and the spin angular momentum associated with circular polarization, the phase shift varies with the rotation angle as

$$\frac{\mathrm{d}\phi}{\mathrm{d}x} = \sigma_{\pm}\frac{\pi}{\Gamma} \quad (5)$$

where $\sigma_{\pm} = \pm 1$ is the photon's spin, corresponding to right and left circular polarization, respectively. Thus, according to equations (4) and (5), the angle of the wakes becomes photon spin-dependent, with an extra phase shift $\Delta\phi$ that can be added or subtracted from the phase shift due to the obliquely incident light. For light impinging at normal incidence, the angle $\gamma$ of the wakes, which was 0° for the slit, becomes non-zero and switches sign by reversing the spin angular momentum of the light.

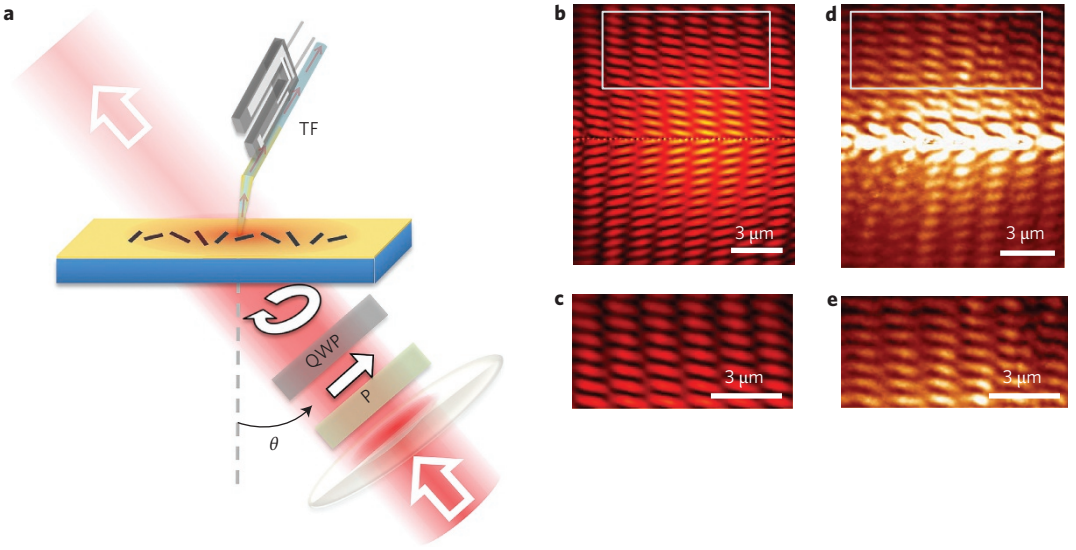


**Figure 5 | Experimental set-up, near-field scanning optical microscopy images for the one-dimensional metamaterial and comparison to analytical model.** **a**, Schematic of the NSOM set-up. A circularly polarized beam is incident at different angles onto the sample. The NSOM signal measured is the interference between the surface plasmons and the transmitted laser light. P, QWP and TF denote the polarizer, quarter waveplate and NSOM tuning fork, respectively. **b**,**d**, Calculated (**b**) and measured (**d**) results using the experimental set-up in **a**, with angle of incidence $\theta = -18°$ (sign denotes anticlockwise, as in **a**). **c**,**e**, Insets of **b** and **d** at the location given by the two white rectangles.

## Analytical model treating each nanoslit as a dipole

The expected SPP intensity distribution far from each antenna can be calculated by using the model discussed above, which approximates the line of apertures by a series of phased dipoles with varying orientation, as given by equation (5). Every antenna on the line can be modelled by a single, in-plane dipole oriented normal to the aperture (Supplementary Section 2). Notice that, for a given observation point on the surface, while the amplitude of the SPP from each antenna depends on the antenna orientation, the SPP wakes result from the coherent sum of the SPPs excited by each nanoslit. Using this dipolar model, we calculated the SPP fields emitted by a linear array of ten periods of apertures rotating at a rate $\Omega = (\pi/1.5\ \mu m)$. These are assumed to be excited by a focused Gaussian beam impinging onto the apertures at normal incidence, that is, with a flat wavefront (Fig. 4a). Under this condition, the coupling efficiency of light to surface wakes is rather low. Around 13% of the incident optical power is coupled at the metallic surface. The efficiency of this launching mechanism can be significantly increased by using a plasmonic resonance, or by changing the incident light beam waist to concentrate more of the power onto the nanoslits (Supplementary Figs 9 and 10).

The results of the calculation in Fig. 4 show that the arrangement of antennas generates SPP wakes that feature parallel alleys of vanishing intensity (dashed line in Fig. 3a). This effect is due to the phase shift introduced by each period, which according to equation (5) varies only from 0 to π. This range occurs because linear antennas oriented at $\alpha$ and $\alpha + \pi$ are equivalent, as can be seen from Fig. 3a. Thus, each period generates an independent plasmon wavefront, tilted as described by equation (4) and π-phase shifted with respect to the wavefronts generated by the two adjacent periods (Fig. 3a). Furthermore, due to destructive interference, zero-intensity alleys are created in the direction normal to the wavefronts. These lines (Fig. 4b) correspond to the low-intensity parallel alleys in Fig. 4d, where the residual intensity is that of the transmitted beam. At normal incidence, the wavefront is spatially homogeneous in the $x$–$y$ plane, so interference with the SPPs produces an intensity distribution where the maximum intensity lines within each alley match the SPP wavefronts. Using the dipolar model we calculated the expected intensity and phase distribution of the surface plasmons (Fig. 4b,c, respectively).

To verify the generation of wakes as predicted by equation (4), we excited the apertures at an angle. To do so, we modified the NSOM set-up to excite the apertures with a circularly polarized focused Gaussian beam at oblique incidence, as shown in Fig. 5a. An example of the experimental NSOM images (Fig. 5d,e) obtained using $\sigma^+$ polarization and comparison with the dipolar model (Fig. 5b,c) are also presented. Interestingly, because the incident beam that interferes with the plasmon field is not impinging at normal incidence, the lines of maximum intensity within each alley are not normal to the propagation direction of the SPP wakes. To accurately measure the angle of the plasmon wakes, we rely on the orientation of the minimum intensity lines, which are parallel to the alleys and wavevectors (Fig. 5). We obtained images for different angles of incidence $\theta$ and spin angular momentum of light, extracted the $\gamma$ angles and compared our results with the theoretically expected angles given by equation (4). The measurements are in excellent agreement with the calculated images and the theoretical expected angles (Fig. 6). By exciting the apertures with light with spin angular momentum, we achieved directional launching of SPPs. Unidirectional on-axis emission[25] (corresponding to $\gamma = 90°$), could also be possible whenever the phase velocity of the RWP along the line matches the phase velocity of SPPs. Interestingly, we also note that an analogue to reversed Cherenkov radiation, previously observed in negative-index metamaterials[14], can be observed in our device simply by switching the spin of the photon for small angles of incidence (Fig. 6b), as the SPP wakes can be made to propagate in the forward or backward direction relative to the incident light.

## Conclusion

Expanding on the Cherenkov description for the case of a slit, where the wake angle is determined by $\sin\gamma = (c_{SPP}/c_{RWP})$, we derive a generalized phase velocity for the RWP of a one-dimensional phased array metamaterial, where $\sin\gamma = c_{SPP}/c_{RWP,gen}$. By substituting in equation (4) and recalling that the phase gradient is given by equation (5), we find that

$$c_{RWP,gen} = \frac{c}{\sin\theta \pm (1/k_0)(\pi/\Gamma)} \quad (6)$$

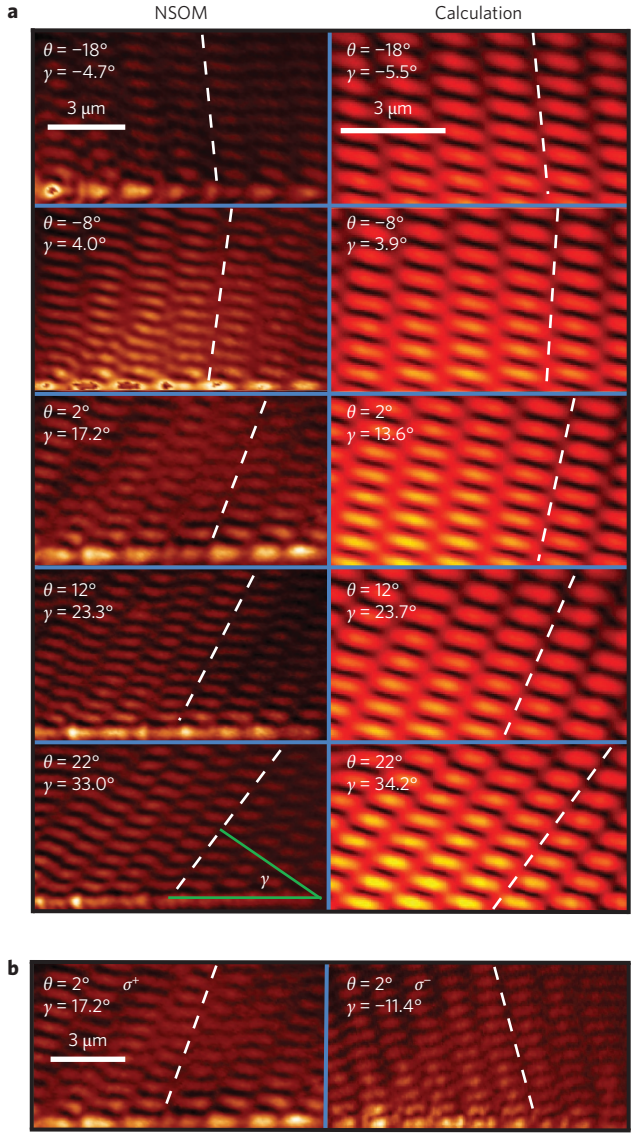


**Figure 6 | Near-field scanning optical microscopy images on the steering of surface plasmon wakes. a**, Side-by-side comparison between NSOM images for different angles of incidence and the calculated interference patterns. The linear array of antenna apertures has a period $\Gamma = 1.5$ μm and the incident beam is $\sigma^+$ polarized. Dashed lines: minimum intensity regions parallel to the alleys. Angles $\gamma$ are obtained from the intersection of the normal to the white dashed lines, as shown in green. **b**, Comparison between $\sigma^+$ and $\sigma^-$ polarization showing that, for small angles, changing the spin angular momentum of the light reverses the direction of the wakes. The standard deviation of the $\gamma$ angle measurements for all experimental images is <2.8°.

From equation (6), we note that by decreasing the phase velocity of the excitation, that is, by increasing the magnitude of the denominator, one could access an interesting new regime in which a propagating polarization wave, with dispersion given by $\omega = c_{RWP,gen}k$, exists along the line of apertures without creating any SPP wakes. Such a subplasmonical regime is connected to the recent work by Sun *et al.* and Qu *et al.*, in which the authors studied the propagation of waves guided along gradient-index metasurfaces and their re-radiation into free space[26–28]. They reported that two-dimensional metasurfaces radiate into free space whenever the moving charges have an effective velocity greater than the speed of light. Below this limit, the waves are confined at the interface. In our structures, analogous driven waves could be confined along a line and generated without coupling to a propagating SPP mode.

In this Article, we have demonstrated that a one-dimensional metamaterial made of rotated nano-apertures etched in a metallic film can arbitrarily control the phase velocity of a RWP propagating along the line formed by the apertures. The phase velocity of the RWP exceeds the SPP phase velocity and results in the creation of SPP wakes. We show that SPPs are excited and constructively interfere via a mechanism analogous to Cherenkov radiation, and we demonstrate that the rotation of the antennas makes the wake direction dependent on spin angular momentum, meaning that the direction of propagation of SPPs could in principle be reversed in real time by rotating a quarter waveplate to change the incident polarization from $\sigma^+$ to $\sigma^-$. This demonstration of SPP wake generation and SPP steering can be further exploited to create new types of plasmonic couplers, such as plasmonic holograms[29] or directional lenses[30,31]. Besides connecting this coupling mechanism with the physics of the Cherenkov effect, our methodology could represent a unique and practical way to test concepts associated with fast travelling perturbations. This work also brings the concepts of leaky wave antennas, previously demonstrated in the millimetre and microwave bands[32], to optical frequencies. Leaky wave antennas have found innovative applications in wavefront engineering, and we expect that these ideas can be exploited to develop similarly impactful applications at optical frequencies.

Received 8 December 2014; accepted 3 June 2015;
published online 6 July 2015

## References

1. Kelvin, W. T. On the waves produced by a single impulse in water of any depth, or in a dispersive medium. *Proc. R. Soc. Lond.* **42,** 80–83 (1887).
2. Landau, L. D. *et al. Electrodynamics of Continuous Media* Vol. 8 (Elsevier, 1984).
3. Veselago, V. G. The electrodynamics of substances with simultaneously negative values of ε and μ. *Physics-Uspekhi* **10,** 509–514 (1968).
4. Grbic, A. & Eleftheriades, G. V. Experimental verification of backward-wave radiation from a negative refractive index metamaterial. *J. Appl. Phys.* **92,** 5930–5935 (2002).
5. Xi, S. *et al.* Experimental verification of reversed Cherenkov radiation in left-handed metamaterial. *Phys. Rev. Lett.* **103,** 194801 (2009).
6. Duan, Z. *et al.* Novel electromagnetic radiation in a semi-infinite space filled with a double-negative metamaterial. *Phys. Plasmas* **19,** 013112 (2012).
7. Smith, S. J. & Purcell, E. M. Visible light from localized surface charges moving across a grating. *Phys. Rev.* **92,** 1069 (1953).
8. Doucas, G. *et al.* First observation of Smith–Purcell radiation from relativistic electrons. *Phys. Rev. Lett.* **69,** 1761 (1992).
9. Luo, C. *et al.* Cerenkov radiation in photonic crystals. *Science* **299,** 368–371 (2003).
10. Casey, K. F., Yeh, C. & Kaprielian, Z. A. Cerenkov radiation in inhomogeneous periodic media. *Phys. Rev.* **140,** B768 (1965).
11. De Abajo, F. J. G. Interaction of radiation and fast electrons with clusters of dielectrics: a multiple scattering approach. *Phys. Rev. Lett.* **82,** 2776 (1999).
12. Adamo, G. *et al.* Light well: a tunable free-electron light source on a chip. *Phys. Rev. Lett.* **103,** 113901 (2009).
13. De Abajo, F. J. G. Optical excitations in electron microscopy. *Rev. Mod. Phys.* **82,** 209 (2010).
14. Duan, Z. *et al.* Reversed Cherenkov radiation in a waveguide filled with anisotropic double-negative metamaterials. *J. Appl. Phys.* **104,** 063303 (2008).
15. Lee, S. Y. *et al.* Role of magnetic induction currents in nanoslit excitation of surface plasmon polaritons. *Phys. Rev. Lett.* **108,** 213907 (2012).
16. Nahpal, P. *et al.* Ultrasmooth patterned metals for plasmonics and metamaterials. *Science* **325,** 594–597 (2009).
17. Yu, N. & Capasso, F. Flat optics with designer metasurfaces. *Nature Mater.* **13,** 139–150 (2014).
18. Genevet, P. & Capasso, F. Flat optics: wavefronts control with Huygens' interfaces. *IEEE Photon. J.* **6,** 1–4 (2014).
19. Yu, N. *et al.* Light propagation with phase discontinuities: generalized laws of reflection and refraction. *Science* **334,** 333–337 (2011).
20. Ni, X. *et al.* Broadband light bending with plasmonic nanoantennas. *Science* **335,** 427–427 (2012).
21. Genevet, P. *et al.* Ultra-thin plasmonic optical vortex plate based on phase discontinuities. *Appl. Phys. Lett.* **100,** 013101 (2012).
22. Shitrit, N. *et al.* Spin-optical metamaterial route to spin-controlled photonics. *Science* **340,** 724–726 (2013).

23. Shitrit, N. *et al.* Rashba-type plasmonic metasurface. *Opt. Lett.* **38,** 4358–4361 (2013).
24. Shitrit, N. *et al.* Spin-controlled plasmonics via optical Rashba effect. *Appl. Phys. Lett.* **103,** 211114 (2013).
25. Lin, J. *et al.* Polarization-controlled tunable directional coupling of surface plasmon polaritons. *Science* **340,** 331–334 (2013).
26. Sun, S. *et al.* Gradient-index meta-surfaces as a bridge linking propagating waves and surface waves. *Nature Mater.* **11,** 426–431 (2012).
27. Sun, S. *et al.* High-efficiency broadband anomalous reflection by gradient meta-surfaces. *Nano Lett.* **12,** 6223–6229 (2012).
28. Qu, C. *et al.* A theoretical study on the conversion efficiencies of gradient meta-surfaces. *Europhys. Lett.* **101,** 54002 (2013).
29. Genevet, P. & Capasso, F. Holographic optical metasurfaces: a review of current progress. *Rep. Prog. Phys.* **78,** 024401 (2015).
30. Lee, S. Y. *et al.* Plasmonic meta-slit: shaping and controlling near-field focus. *Optica* **2,** 6–13 (2015).
31. Wintz, D. *et al.* Holographic metalens for switchable focusing of surface plasmons. *Nano Lett.* **5,** 3585–3589 (2015).
32. Jackson, D. R., Caloz, C. & Itoh, T. Leaky-wave antennas. *Proc. IEEE* **100,** 2194–2206 (2012).

## Acknowledgements

The authors thank T. Mansuripur, H. Galinski, M.A. Kats, J.P.B. Mueller and R. Zhang for discussions. The authors acknowledge Nanonics Ltd and MPD S.r.l. for support with the near-field set-up and photon detection, respectively. The authors acknowledge support from the Harvard Nanoscale Science and Engineering Center (NSEC; contract no. NSF/PHY 06-46094), from the Science and Engineering Research Council (SERC grant no. 1426500053) and the Center for Nanoscale Systems (CNS) at Harvard University, which is a member of the National Nanotechnology Infrastructure Network (NNIN). This work was supported by a National Science Foundation Early-Concept Grant for Exploratory Research (grant no. ECCS-1347251) and by the Air Force Office of Scientific Research (grant no. FA9550-12-1-0289).

## Author contributions

P.G., D.W., A.A., A.S. and R.B. developed the theoretical descriptions. P.G. fabricated the devices. D.W., A.A. and P.G. conducted the experiments and analysed the results. A.A. and D.W. implemented the analytical model. P.G. and F.C. directed the research. P.G., D.W. and F.C. wrote the paper, with contributions from the other authors. P.G., D.W. and A.A. contributed equally to this work.

## Additional information

Supplementary information is available in the online version of the paper. Reprints and permissions information is available online at www.nature.com/reprints. Correspondence and requests for materials should be addressed to P.G. and F.C.

## Competing financial interests

The authors declare no competing financial interests.